

# Birth and death of a single quantum of vibration

Santiago Tarrago Velez,<sup>1</sup> Kilian Seibold,<sup>1</sup> Nils Kipfer,<sup>1</sup> Mitchell D. Anderson,<sup>1</sup> Vivishek Sudhir,<sup>2</sup> and Christophe Galland<sup>1</sup>

<sup>1</sup>*Institute of Physics, Ecole Polytechnique Fédérale de Lausanne (EPFL), CH-1015 Lausanne, Switzerland*

<sup>2</sup>*LIGO Laboratory, Massachusetts Institute of Technology, Cambridge, MA 02139, USA*

(Dated: July 8, 2022)

**A single quantum of excitation of a mechanical oscillator is a textbook example of the principles of quantum physics. Mechanical oscillators, despite their pervasive presence in nature and modern technology, do not generically exist in an excited Fock state. In the past few years, careful isolation of GHz-frequency nano-scale oscillators has allowed experimenters to prepare such states at milli-Kelvin temperatures. These developments illustrate the tension between the basic predictions of quantum mechanics that should apply to all mechanical oscillators existing even at ambient conditions, and the complex experiments in extreme conditions required to observe those predictions. We resolve the tension by creating a single Fock state of a vibration mode of a crystal at room temperature using a technique that can be applied to any Raman-active system. After exciting a bulk diamond with a femtosecond laser pulse and detecting a Stokes-shifted photon, the 40 THz Raman-active internal vibrational mode is prepared in the Fock state  $|1\rangle$  with 98.5% probability. The vibrational state is read out by a subsequent pulse, which when subjected to a Hanbury-Brown-Twiss intensity correlation measurement reveals the sub-Poisson number statistics of the vibrational mode. By controlling the delay between the two pulses we are able to witness the decay of the vibrational Fock state over its 3.9 ps lifetime at room temperature. Our technique is agnostic to specific selection rules, and should thus be applicable to any Raman-active medium, opening a new generic approach to the experimental study of quantum effects related to vibrational degrees of freedom in molecules and solid-state systems.**

The observation of inelastic scattering of photons from ensembles of atomic-scale particles was an early triumph of quantum theory. Within half a decade, experiments by Compton [1] and Raman [2] showed that photons can exchange energy and momentum with material particles in the manner described by quantum mechanics. At optical frequencies, Raman scattering, the dominant effect, is an expression of the universal idea that a mechanical vibration phase-modulates the outgoing light, resulting in two scattered sidebands (Fig. 1a,b). In a quantum description, the upper (“anti-Stokes”) sideband arises from the annihilation of a quantum of vibration, while the lower (“Stokes”) arises from its creation (Fig. 1c).

Observing true quantum signatures of the vibration itself has proved far more elusive. On the one hand, internal vibrational modes of crystals and molecules with oscillation frequencies in the 10-100 THz range – the subject of Raman spectroscopy – ubiquitously and naturally exist in their quantum ground state at room temperature; but unless they are individually addressed and resolved within their coherence time, the ensemble average over uncontrolled vibrational modes precludes the observation of their quantum behavior. Despite the challenge, a Raman-active vibration featuring a specific form of internal nonlinearity was prepared in a squeezed state by optical excitation [3], while polarization-selective Raman interactions were used to prepare an entangled state of two vibrational modes by projective measurements [4]. On the other hand, nano-fabricated mechanical oscillators can be susceptible to a universal radiation pressure interaction with light, especially when interacting with

the intense fields stored in an optical cavity [5]. However, their relatively low frequency (MHz-GHz) means that thermal energy at room temperature is larger than the energy of a single vibrational quantum, making quantum state manipulation difficult or impossible under ambient conditions. Precise measurements of mechanical motion at room temperature has recently revealed quantum characteristics of the underlying radiation pressure interaction [6, 7]. But it is only through deep cryogenic operation that quantum states of motion of nano-scale oscillators have been prepared in the last years [8–12]. Thus, the quest to prepare quantum states of commonly available mechanical oscillators at ambient conditions remains largely open.

Here we prepare a non-classical state of the internal vibrations of a diamond crystal at room temperature. In a scheme inspired by the DLCZ protocol [13, 14], a femtosecond laser pulse (the “write” pulse hereafter) first creates an excitation from the ambient motional ground state with a probability  $p \ll 1$  (see fig. 1c). Detection of the emitted Stokes photon heralds the success of this step, while choice of the spectral window for detection fixes the specific vibrational mode of the system under study. To verify that only a single quantum of vibration was excited, a second laser pulse (the “read” pulse) retrieves it as an anti-Stokes photon. The probability of having two or more anti-Stokes photons, and therefore two or more quanta of vibrations, is obtained by performing a Hanbury-Brown-Twiss (HBT) intensity correlation measurement on the anti-Stokes photons conditioned on the heralding signal [15, 16]. In fact, we observe sub-

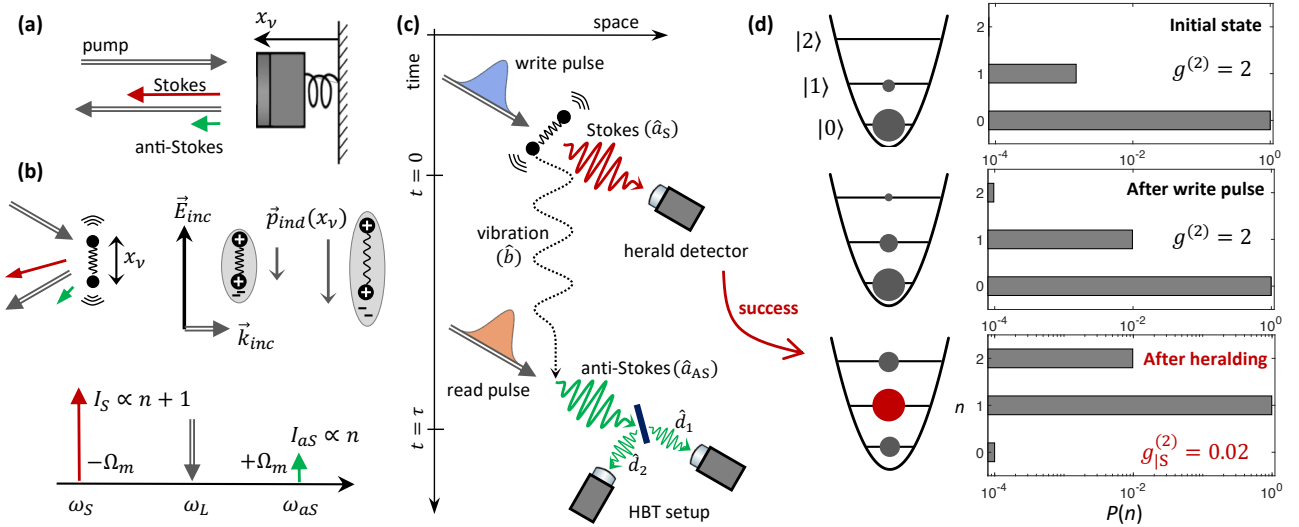


FIG. 1. **Concept of the experiment.** (a) When monochromatic light reflects from an oscillating mirror, it acquires two Raman sidebands due to phase modulation (to first order in interaction strength). (b) When light interacts with a polarizable oscillator, whose induced polarization  $\vec{p}_{ind}$  depends on its internal coordinate  $x_v$ , it undergoes a phase modulation at the oscillator frequency, leading to the appearance of Stokes and anti-Stokes Raman sidebands in the scattered light. The anti-Stokes/Stokes intensity ratio is proportional to  $\frac{\bar{n}}{\bar{n}+1}$  where  $\bar{n}$  is the mean excitation number (or occupancy) of the vibrational mode. (c) Time evolution of a single repetition of the experiment showing the interaction of the write pulse, the subsequent detection of Stokes photons for heralding, and the final read pulse followed by measurement of two-photon correlation in the emitted anti-Stokes light. (d) Evolution of the probability  $P(n)$  of finding the vibrational mode in the  $n^{\text{th}}$  energy eigenstate during the different steps. The system is initially in a thermal state with  $\bar{n} = 1.5 \cdot 10^{-3}$  (for a mode frequency of 40 THz at 295 K). After the write pulse, the marginal state of the vibration is also thermal with  $\bar{n} = \frac{p}{1-p} = 10^{-2}$  in this example (here  $p$  is the interaction probability). Finally, after heralding, the distribution becomes peaked at  $n = 1$ . The residual vacuum component is due to detection noise. For each distribution, we give the corresponding value of the vibrational mode's intensity correlation function  $g^{(2)}$ .

Poissonian statistics of the vibrational state via such a heralded intensity correlation measurement, a result consistent with having prepared the Fock state  $|1\rangle$  of the vibrational mode (the first excited energy eigenstate). Finally by changing the delay between the write and read pulses we probe the decay of the single vibrational quantum, with approximately 200 fs resolution.

In contrast to previous quantum optics experiments on Raman-active vibrational modes that were restricted to molecular or crystal structures exhibiting particular polarization rules [4, 17–22] or vibrational nonlinearities [3], our technique is agnostic to these details, and can be employed on any Raman-active subject. It opens a plethora of opportunities to study vibrational quantum states and dynamics in other crystals and in molecules, and can readily be extended to create vibrational two-mode entangled states [23] to test the violation of Bell inequalities [24, 25] at room-temperature in a number of widely available systems.

## Theoretical description

The nonlinear Raman interaction between a single vibrational mode and an optical field leads to the creation of an anti-Stokes (Stokes) photon commensurate with the destruction (creation) of a vibrational quantum. In our

experiment the Raman interaction is driven by an optical field that may either be a “write” (w) or “read” (r) pulse defined by the spatial and temporal mode of a mode-locked laser whose beam is focused onto the sample. These two incident fields are described by the annihilation operators  $\hat{a}^{w,r}$ . The interaction leads to the generation of Stokes and anti-Stokes photons whose spatial mode is post-selected by a single-mode optical fiber. These Stokes/anti-Stokes fields are modeled by annihilation operators  $\hat{a}_S^{w,r}$  ( $\hat{a}_{AS}^{w,r}$ ). Due to conservation of energy and momentum in the Raman scattering process, the detection of these scattered fields defines a single spatio-temporal mode of the vibration that is the subject of the experiment, and which we describe by its annihilation operator  $\hat{b}$ . The Raman interaction is modeled by the Hamiltonian [26],

$$\hat{H}_{int}^{w,r} = i\hbar \left[ G_S^{w,r} \hat{a}^{w,r} \hat{b}^\dagger (\hat{a}_S^{w,r})^\dagger + G_{AS}^{w,r} \hat{a}^{w,r} \hat{b} (\hat{a}_{AS}^{w,r})^\dagger \right] + \text{h.c.}, \quad (1)$$

where the coupling rates  $G_S^{w,r}$  and  $G_{AS}^{w,r}$  are complex numbers related to the Raman activity of the vibrational mode.

None of the four processes described by eq. (1) is resonant since we work at photon energies well below the band gap of diamond (5.47 eV). However, because we

spectrally filter and detect only the two modes  $a_S^w$  and  $a_{AS}^r$  all essential results of our measurements can be described by the Hamiltonian

$$\hat{H}_{\text{int}}^{w,r} = i\hbar \left[ g_S^w \hat{b}^\dagger \hat{a}_S^\dagger + g_{AS}^r \hat{b} \hat{a}_{AS}^\dagger \right] + \text{h.c.}, \quad (2)$$

where we defined the effective interaction rate,  $g_{S,AS}^{w,r} \equiv G_{S,AS}^{w,r} \sqrt{n_p^{w,r}}$ , corresponding to a classical excitation for the write/read pulses with  $n_p^{w,r}$  photons per pulses, and used the shorter notation  $\hat{a}_S \equiv \hat{a}_S^w$ ,  $\hat{a}_{AS} \equiv \hat{a}_{AS}^r$ . In fact, this scenario is equivalent to the linearized radiation-pressure interaction [5], or Raman processes in atomic ensembles [13], where an optical cavity (in the former instance) or electronic resonance (in the latter) suppresses non-resonant terms.

Note that the Hamiltonian in eq. (2) neglects higher order interactions, in particular the creation of correlated Stokes/anti-Stokes pairs during a single pulse (write or read) via four-wave mixing [27–32]. The photon flux due to this higher-order interaction constitutes an effective background noise on the photodetectors since filters in the experiment prevent coincidence counts from this spurious emission. Other extraneous sources of photons, such as from residual  $\chi^{(3)}$  nonlinearities, or fluorescence, also lead to an excess background noise. The spontaneous Stokes signal scales linearly with laser power and is proportional to  $n_p^w(\bar{n} + 1) \approx n_p^w$ , where  $\bar{n}$  is the average occupation of the vibrational mode. In our experimental conditions, it is much stronger than any of the parasitic processes described above, so that the fidelity of the heralded state is only marginally affected by noise. However, the anti-Stokes signal, being proportional to  $n_p^r \bar{n}$ , is significantly weaker, so that the noise cannot be neglected in this case. The measured normalized probability of detecting two anti-Stokes photon should therefore be considered as an upper-bound for the corresponding probability of having two vibrational quanta. In the calculations presented below, the noise terms are accounted for in order to faithfully describe the experiment.

**Write operation** The first step in an iteration of the experiment is the excitation of the vibrational mode by a write pulse. The resulting dynamics of the vibrational and Stokes modes is governed by  $H_{\text{int}}^w = i\hbar g_S^w \hat{b}^\dagger \hat{a}_S^\dagger + \text{h.c.}$ , which has the form of a two-mode squeezing interaction, and leads to the creation of maximally correlated pairs of vibrational and Stokes excitations. When both modes are initially in the vacuum state  $|\text{vac}\rangle$ , the final state after the write pulse is [16],

$$|\Psi\rangle_{S,b} = \sqrt{1-p} \sum_{n=0}^{\infty} \sqrt{p^n} |n, n\rangle_{S,b} \quad (3)$$

where  $|n, n\rangle_{S,b} \equiv \frac{(\hat{b}^\dagger \hat{a}_S^\dagger)^n}{n!} |\text{vac}\rangle$ . For the simple situation of a constant interaction switched on for a duration  $T_w$ ,

the probability of exciting the state  $|1, 1\rangle$  is given by,  $p = \tanh^2(g_S^w T_w)$ ; in the general case,  $T_w$  is the effective interaction time defined by the equivalent square pulse that carries the same energy as that of the real pulse. Ideally, when at least one Stokes photon is detected, the (conditional) state of the vibrational mode becomes (see Supplementary information),  $\rho_{b|S} \approx |1\rangle\langle 1| + p|2\rangle\langle 2|$ , in the limit where  $p \ll 1$ ; crucially, the vacuum component in  $|\Psi\rangle_{S,b}$  has been eliminated based on the presence of a Stokes photon. Dark noise in real photodetectors (modeled as a probability  $\pi_0$  per pulse) prevents unambiguous discrimination of the vacuum contribution. However, when the total Stokes signal is larger than the dark noise, it can be shown (see Supplementary information) that the resulting conditional state,

$$\hat{\rho}_{b|S} \approx \frac{\pi_0}{2\eta p} |0\rangle\langle 0| + |1\rangle\langle 1| + p|2\rangle\langle 2|, \quad (4)$$

is still the pure Fock state  $|1\rangle$  to a high degree. Here  $\eta$  is the detection efficiency of the Stokes field, and  $\eta p$  is the Stokes detection probability. The signal-to-noise ratio in the Stokes photodetector  $\eta p/\pi_0$  is larger than  $10^4$  in our experiment.

**Read operation** Once the Stokes photon is detected, a second pulse – the read pulse – is used to retrieve the conditional state of the vibrational mode. The dynamics of the anti-Stokes field induced by the read pulse is described by the Hamiltonian  $H_{\text{int}}^r = i\hbar g_{AS}^r \hat{b} \hat{a}_{AS}^\dagger + \text{h.c.}$ , which represents a beam splitter interaction between the anti-Stokes and vibrational modes. For an effective interaction time  $T_r$ , the emitted anti-Stokes field is given by the input-output relation,

$$\hat{a}_{AS}(T_r) = \cos(\theta) \hat{a}_{AS}(0) + \sin(\theta) \hat{b}, \quad (5)$$

where,  $\theta \equiv g_{AS}^r T_r$ . The mode  $\hat{a}_{AS}(0)$  describes the input anti-Stokes mode (before the read pulse) which is in the vacuum state.

The crucial aspect of the read operation is that the emitted anti-Stokes field faithfully reflects the number statistics of the vibrational mode. In fact, from eq. (5),  $\langle : (\hat{a}_{AS}^\dagger \hat{a}_{AS})^n : \rangle = \sin^{2n}(\theta) \langle : (\hat{b}^\dagger \hat{b})^n : \rangle$ , for any integer  $n \geq 1$  (here  $::$  denotes normal ordering). This relation expresses the fact that photon counting is insensitive to vacuum noise (in stark contrast to linear detection of the field [33]), so that normalized moments of the photon number of the anti-Stokes field faithfully represent the statistics of the vibrational mode excitation number.

**Statistics of the heralded intensity correlation** Performing the two operations presented above enables the preparation and unambiguous characterization of a vibrational Fock state. Consider that the Stokes field, the vibration, and the anti-Stokes field is in the joint state  $|\Psi\rangle_{S,b,AS}$  representing the state of knowledge when at

time  $t = 0$  a Stokes photon has been detected, a time  $t$  has elapsed between the write and read operation, and subsequently the anti-Stokes field has been detected in coincidence. This heralded coincidence event is represented by the measurement map,

$$|\Psi\rangle_{\text{S,b,AS}} \mapsto \hat{d}_2^\dagger(t)\hat{d}_1^\dagger(t)\hat{a}_\text{S}(0)|\Psi\rangle_{\text{S,b,AS}},$$

while  $\hat{d}_{1,2}$  are the operators denoting the anti-Stokes field split at a beam-splitter (see fig. 1c). The probability of this triple coincidence defines the conditional intensity correlation, and is thus proportional to,  $\langle \hat{a}_\text{S}^\dagger(0)\hat{d}_1^\dagger(t)\hat{d}_2^\dagger(t)\hat{d}_2(t)\hat{d}_1(t)\hat{a}_\text{S}(0) \rangle$ , where we have used the linearity of quantum mechanics to extend the definition to mixed states as well. Suitably normalizing the expression [34] allows us to define the conditional intensity correlation,

$$g_{\text{AS|S}}^{(2)}(t) \equiv \frac{\langle \hat{a}_\text{S}^\dagger(0)\hat{d}_1^\dagger(t)\hat{d}_2^\dagger(t)\hat{d}_2(t)\hat{d}_1(t)\hat{a}_\text{S}(0) \rangle}{\prod_i \left[ \langle \hat{a}_\text{S}^\dagger(0)\hat{d}_i^\dagger(t)\hat{d}_i(t)a_\text{S}(0) \rangle \langle \hat{a}_\text{S}^\dagger(0)\hat{a}_\text{S}(0) \rangle^{-1/2} \right]}.$$

The fields  $\hat{d}_{1,2}$  whose second order (cross) correlations are measured can be expressed in terms of the anti-Stokes field  $\hat{a}_\text{AS}$ , which in turn can be expressed in terms of the vibration (via eq. (5)); since intensity correlations do not respond to the vacuum, the open port of the beam-splitter used in the intensity correlation plays no part, and the conditional correlation above can be written as,

$$g_{\text{AS|S}}^{(2)}(t) = \frac{\langle \hat{a}_\text{S}^\dagger(0)\hat{b}^\dagger(t)\hat{b}^\dagger(t)\hat{b}(t)\hat{b}(t)\hat{a}_\text{S}(0) \rangle}{\langle \hat{a}_\text{S}^\dagger(0)\hat{a}_\text{S}(0) \rangle^{-1} \langle \hat{a}_\text{S}^\dagger(0)\hat{b}^\dagger(t)\hat{b}(t)\hat{a}_\text{S}(0) \rangle^2}. \quad (6)$$

After the detection of a Stokes photon (i.e. for  $t > 0$ ), the state of the vibrational mode (eq. (4)) has disentangled from that of the Stokes mode, so that expectation values of products of operators in their joint state factorize into products of expectation values; using this fact, the above equation reduces to,

$$g_{\text{AS|S}}^{(2)}(t > 0) = \frac{\langle \hat{b}^\dagger(t)\hat{b}^\dagger(t)\hat{b}(t)\hat{b}(t) \rangle}{\langle \hat{b}^\dagger(t)\hat{b}(t) \rangle^2} = g_b^{(2)}. \quad (7)$$

That is, the conditional intensity correlation of the anti-Stokes field gives the intensity correlation of the vibrational mode. Immediately after the write pulse (i.e.  $t = 0$ , and in the limit of a small probability  $p$  of exciting a vibrational Fock state, explicit evaluation of eq. (6) on the state  $|\Psi\rangle_{\text{S,b}}$  of eq. (3) yields

$$g_{\text{AS|S}}^{(2)}(0) \approx \frac{4P(2,2)}{P(1,1)} = 4p \quad (8)$$

where  $P(n,n)$  is the probability that an  $n$ -pair state between the vibrational mode and the Stokes field was created.

In our experiment we measure the number of the events  $N_{d_1,d_2,a_\text{S}}$  where photons were detected simultaneously in modes  $d_1, d_2$ , and  $a_\text{S}$  (i.e. triple coincidence), and normalize it to the product of the number of events  $N_{d_i,a_\text{S}}$  ( $i = 1, 2$ ) where photons are detected simultaneously in the Stokes mode and one of the downstream detectors (i.e. a two-fold coincidence); we thus measure [15],

$$\alpha \equiv \frac{N_{d_1,d_2,a_\text{S}}N_{a_\text{S}}}{N_{d_1,a_\text{S}}N_{d_2,a_\text{S}}}. \quad (9)$$

It is important to note that  $\alpha$  is not equivalent to  $g_{\text{AS|S}}^{(2)}$  in general. More precisely, if the detection efficiency of the herald mode  $a_\text{S}$  is  $0 < \eta_\text{S} \leq 1$  (which we model as a beam splitter with transmittance  $\eta_\text{S}$  placed before the detector) we find (see Supplementary information)

$$\alpha \approx (4 - 2\eta_\text{S}) \frac{P(2,2)}{P(1,1)} = (4 - 2\eta_\text{S})p. \quad (10)$$

Thus, in the limit of a low detection efficiency of Stokes photons (i.e.  $\eta_\text{S} \ll 1$ ) we have that  $\alpha = g_{\text{AS|S}}^{(2)}$ .

## Results

**Setup and measurement procedure** Our experimental setup is an upgraded version of that presented in ref. [35]. Two synchronized laser pulse trains at 810 nm and 695 nm of duration  $\Delta t \approx 100$  fs are produced by a Ti:Sa oscillator (Tsunami, Spectra Physics, 80 MHz repetition rate) and a synchronously pumped frequency-doubled optical parametric oscillator (OPO-X fs, APE Berlin), respectively. The write pulses are provided by the OPO, while the Ti:Sa provides the read pulses, which are passed through a delay line before being overlapped with the OPO output on a dichroic mirror. The sample is a synthetic diamond crystal ( $\sim 300 \mu\text{m}$  thick, from Lake-Diamond) cut along the (100) crystal axis and is probed in transmission using two microscope objectives (numerical aperture 0.8 and 0.9). The laser light is blocked using long-pass and short-pass tunable interference filters (Semrock), leaving only a spectral window of transmission for the Stokes signal from the write pulse (mode  $a_\text{S}$ ) and the anti-Stokes signal from the read pulse (mode  $a_\text{AS}^\text{r}$ ). The transmission is collected in a single mode fiber (for spatial mode filtering) and then the two signals are separated with a tunable long-pass filter used as a dichroic mirror. After an additional band-pass filter each signal is coupled into a multi-mode fiber; subsequently, the Stokes field is sent to a single photon avalanche photodiode (SPAD, Excelitas SPCM), while the anti-Stokes field is split at a 50:50 fiber beam-splitter and directed onto two SPADs. The three SPADs are then connected to a coincidence counter (PicoQuant TimeHarp 260).

The statistics of the required coincidence events is assembled from the saved time tags of those events where a click in one of the anti-Stokes channels was preceded by a click in the Stokes channel. This allows us to find

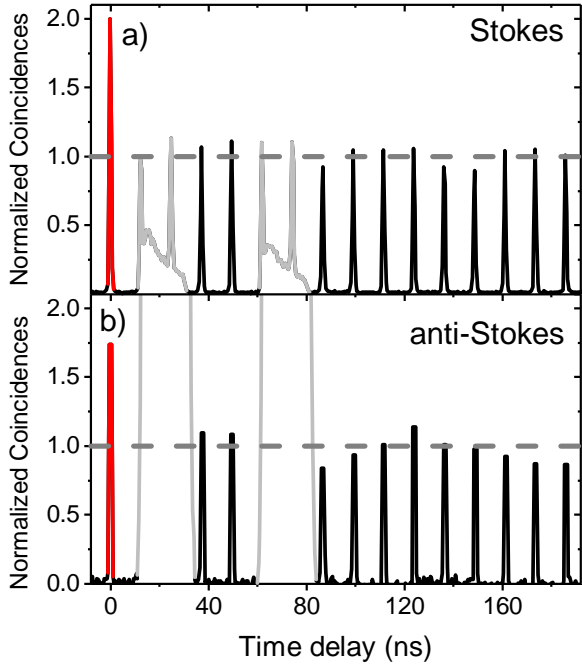


FIG. 2. **Unconditional Stokes and anti-Stokes correlations.** Two-photon coincidence histograms of the (a) Stokes field  $\hat{a}_S$  (write pulse energy 60 pJ, acquisition time 10 min) and (b) anti-Stokes field  $\hat{a}_{AS}$  (read pulse energy 372 pJ, acquisition time 1 hr). For panel (b) the coincidences are recorded between the detectors measuring  $\hat{d}_1$  and  $\hat{d}_2$  of Fig. 1b and the write pulse is blocked. For the measurement in panel (a), a beam splitter is added on the path of mode  $\hat{a}_S$  (Fig. 1b). The time delay between each peak corresponds to the repetition period of the experiment ( $\approx 12.5$  ns) and the red trace highlights the zero-delay component. After normalizing by the average number of accidental coincidences (the peaks traced in black) the value at zero time delay represents the intensity correlation of the Stokes and anti-Stokes fields, namely  $g_S^{(2)} = 2.0 \pm 0.1$  and  $g_{AS}^{(2)} = 1.73 \pm 0.11$ . We trace in gray the regions of the histograms (omitted in the analysis) affected by spurious counts from cross-talk between the two detectors arising from hot-carrier-induced photons in one detector [36] that falls on the other detector, triggering a “false” coincidence.

heralded coincidence events (within the same laser repetition), as well as to build a delay histogram using the Stokes channel as the start and either of the anti-Stokes channels as the stop; thus all relevant coincidences required to estimate  $\alpha$  are available.

**Ambient thermal state** We start by verifying that following the write pulse the Stokes field is well described by the state of eq. (3): when marginalized over the state of the vibrational mode, the Stokes field is thermal. Indeed, we find in Fig. 2a that the intensity correlation function of the Stokes field at zero time delay is  $g_S^{(2)}(0) = 2$ , con-

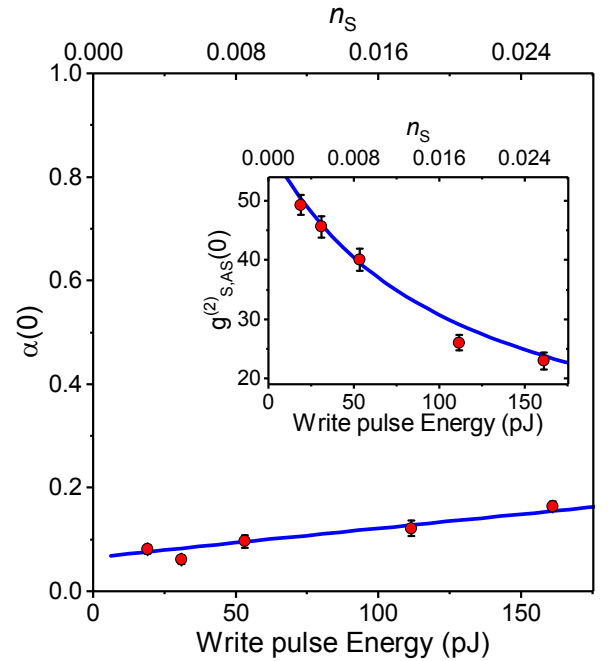


FIG. 3. **Sub-Poisson anti-Stokes statistics.** Dependence on the write pulse energy and on the estimated probability of creating at least one Stokes photon per pulse,  $n_S = \frac{P}{1-P}$ , of the heralded vibrational statistics. The normalized Stokes–anti-Stokes correlations are shown as an inset. The write–read pulse delay is fixed at zero and the read pulse energy at 322 pJ. Statistical error bars are obtained from the square root of the total number of events. Blue lines are models (see Supplementary Information), using the estimated detection efficiency (10 %) and a relative efficiency of the read process (compared to the Stokes emission cross-section) of 30 % as the only two adjustable parameters (common to both panels).

sistent with a thermal state. Similarly, in the absence of the write operation, the anti-Stokes signal should reflect the thermal statistics of the vibrational mode. To check this, we measure the (unconditional) intensity correlation of the anti-Stokes mode, shown in fig. 2b. The value of  $g_{AS}^{(2)}(0) = 1.73 \pm 0.11$ , is slightly lower than the expected value of 2 for a single mode thermal state, but higher than the value  $1 + \frac{1}{N}$  for a thermal state of  $N > 1$  modes [37]. We attribute this discrepancy to the noise in the anti-Stokes channel coming from degenerate four-wave mixing in the sample (which includes the second-order Stokes–anti-Stokes process [29] discussed earlier). We thus confirm that our experiment is probing a single vibrational mode originally in a thermal state, and that the result of the write operation is well described by the two-mode squeezed state of eq. (3).

**Fock state preparation** In order to prepare the vibrational mode in a Fock state, we use a write pulse, and

herald the success of this operation by detecting a Stokes photon. When the subsequent anti-Stokes photons, stimulated by a read pulse, are subjected to intensity correlation measurements, we find that  $\alpha(0) \approx g_{\text{AS}|\text{S}}^{(2)}(0) < 1$ , as shown in fig. 3 (main panel). Thus, the conditional anti-Stokes field exhibits sub-Poissonian statistics. But since we know that the anti-Stokes field is faithful to the vibrational state, and specifically that  $g_{\text{AS}|\text{S}}^{(2)} = g_b^{(2)}$ , we are able to conclude that the vibrational mode must be sub-Poissonian. From the value of  $\alpha(0) \approx 0.06$  at the lowest powers of the write pulse, the known detection efficiency of the Stokes field  $\eta \approx 10\%$ , and our theoretical model, we are able to estimate the probability of having excited the Fock state  $|1\rangle$  to be (eq. (10)),  $1 - p \approx 98.5\%$ .

With increasing power of the write pulse, mixtures of states higher up in the Fock ladder are excited. As shown in fig. 3, the sub-Poisson character of  $\alpha$  decreases with increasing pump power, as expected from the simple model  $\alpha(0) \propto p = \tanh^2(g_S^w T_w) \approx (g_S^w T_w)^2 \propto n_p^w$ ; in tandem, the Stokes–anti-Stokes correlation reduces as  $1/n_p^w$ . These trends are consistent with increasing probability of exciting two or more vibrational quanta [37, 38] (see Supplementary Information for details).

**Fock state dynamics** The decay of the excited vibrational Fock state can be probed by allowing it to evolve freely after the write pulse. In the experiment, we do this by employing a variable optical path length to impose a time delay  $t$  between the write and read pulses. Figure 4 summarizes the observed time-dependence of the excited Fock state. When the write and read pulses overlap ( $t = 0$ ), we observe that the Stokes–anti-Stokes correlation  $g_{\text{S,AS}}^{(2)}(0) \approx 30$ , consistent with the generation of a highly entangled Stokes–vibration state (eq. (3)). Simultaneously,  $\alpha(0)$  which reflects the intensity correlation of the conditioned vibrational state (eq. (4)) indicates sub-Poissonian statistics of the vibrational mode ( $\alpha(0) \approx 0.11$ ). The vibrational mode is prepared in the Fock state  $|1\rangle$ .

Subsequent iterations of the experiment probe the vibrational state after a time delay, demonstrated here for the first time. Figure 4a shows the decay of the Stokes–anti-Stokes correlation. The initial value  $g_{\text{S,AS}}^{(2)}(0)$  quantifies the degree to which the Stokes field and vibrational mode are correlated by the write operation; at later times  $t > 0$ , after the Stokes field is detected,  $g_{\text{S,AS}}^{(2)}(t) \propto \langle \hat{b}^\dagger(t) \hat{b}(t) \rangle$ , so that the data in fig. 4a allows us to infer the decay rate  $\tau_m = 3.9 \pm 0.3$  ps (bounds for 95% confidence). (Note that the model in fig. 4a shows the ideal prediction convolved with the known instrument response function modeled as a gaussian with a 200 fs standard deviation.) In parallel, as shown in fig. 4b,  $\alpha(t)$  mirrors this evolution, starting at  $\alpha(t < 0) = 1.9 \pm 0.6$  (thermal state), dropping to  $\alpha(0) = 0.11 \pm 0.01$  at zero delay (Fock state), and then returning toward its equilib-

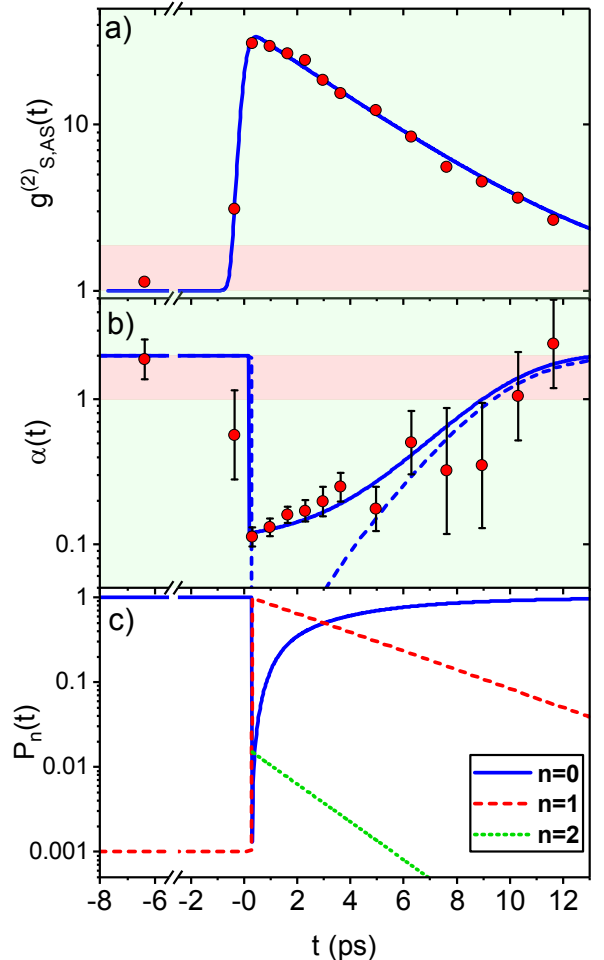


FIG. 4. **Decay of vibrational Fock state.** Measured Stokes–anti-Stokes correlations (red in panel (a)), and heralded vibrational mode intensity correlation (red in panel (b)), decaying with write–read time delay. The measurements are taken with a pulse energy of 62 pJ in the write pulse and 409 pJ in the read pulse, with an acquisition time of 1 hr for all points except the one at  $-6.3$  ps, which was acquired for 8 hr. Statistical error bars are obtained from the square root of the total number of events detected in each case. Red shows measured data and blue shows model (see text for details). Since the decay of  $g_{\text{S,AS}}^{(2)}(t)$  follows the energy decay of the vibrational mode, an exponential fit yields the vibrational lifetime  $\tau_m = 3.9 \pm 0.3$  ps. This value is used in panel (b) to overlay the no-free-parameter model shown in blue. Green bands in panels (a,b) show the region where a non-classical model is required to explain the observations; red bands indicate where a classical model suffices. (c) Fock state distribution of the conditional vibrational mode inferred from data in panel (b).

rium value as the prepared vibrational Fock state thermalizes with its environment. (The larger uncertainty in the data at long and at negative delays is due to the reduced rate of coincidences, because of the small thermal occupancy,  $\bar{n} \approx 1.5 \cdot 10^{-3}$ , of the vibrational mode.) This

behaviour is captured by a simple model (shown in blue in fig. 4b), based on the fact that  $\alpha(t)$  is the intensity correlation of the vibrational mode (eq. (7)) – which can be calculated using an open quantum system model for the vibrational mode – together with a contribution from background noise in the anti-Stokes field (see Supplementary Information),

$$\alpha(t) \approx \frac{2}{P_1(0)} \left[ 1 - \frac{1}{(1 + \bar{n}(e^{t/\tau_m} - 1))^2} \right] + \alpha_0, \quad (11)$$

where  $P_1(0) \approx 0.985$  is the probability of having created the vibrational Fock state  $|1\rangle$  conditioned upon the detection of a Stokes photon, and  $\alpha_0 \approx 0.08$  is the (square of the) phonon-equivalent noise in the anti-Stokes field. The decay of sub-Poisson statistics of the vibrational mode is consistent with the decay of the Fock state  $|1\rangle$ .

The measured decay of the conditional intensity correlation, in conjunction with a decoherence model, can be used to extract the number distribution  $P_n(t)$  of the conditional vibrational state (see Supplementary Information) – the probability to find the vibrational mode in the Fock state  $|n\rangle$  at time  $t$  after a click on the Stokes detector. This projection is plotted in Fig. 4c. Noteworthy is the high purity of the conditional vibrational state with respect to the Fock state  $|n=1\rangle$ , since its normalized second order correlation is  $\frac{2P_2}{P_1^2} \approx 0.02$ . This is much lower than the measured parameter  $\alpha \approx 0.1$  (because the background noise impinging on the anti-Stokes detectors affects  $\alpha$ ) and highlights the potential of the technique to produce high-purity single photon states provided that the contribution of other non-linearities is mitigated, for example by engineering the local density of states of the electromagnetic field around the vibrational mode [39].

**Conclusion** We have demonstrated for the first time that a high-frequency Raman-active vibrational mode can be prepared in its  $n=1$  Fock state at room temperature, and measured via heralded intensity correlations. These measurements confirm the sub-Poissonian statistics of the generated state. We could further probe the decay of the vibrational Fock state, akin to similar measurements on microwave photons [40, 41].

This research opens a door to the study of quantum effects in the vibrational dynamics of Raman-active modes in immobilized molecules [42], liquids, gases [43–45] and solid-state systems. Vibrational states in Raman-active solid-state systems at room temperature may even be viable candidates for quantum technology if the coherence time could be improved. For example, vibrational modes may be used as a buffer memory to produce heralded single photons with an arbitrary choice of the herald and signal wavelengths and/or bandwidths; this would alleviate the stringent requirements on the overlap between pulses. Here, the challenge is to increase

the readout efficiency, possibly using small-mode volume optical or plasmonic cavities [39, 46, 47], or resonant Raman scattering [48, 49]. If successful, this would also realize a quantum coherent interface for frequency conversion at the single photon level, generalizing recent results [21] to a broader class of vibrational systems.

- 
- [1] A. H. Compton, “A quantum theory of the scattering of x-rays by light elements,” *Phys. Rev.* **21**, 483 (1923).
  - [2] C. V. Raman and K. S. Krishnan, “A new type of secondary radiation,” *Nature* **121**, 501 (1928).
  - [3] G. A. Garrett, A. G. Rojo, A. K. Sood, J. F. Whitaker, and R. Merlin, “Vacuum Squeezing of Solids: Macroscopic Quantum States Driven by Light Pulses,” *Science* **275**, 1638–1640 (1997).
  - [4] K. C. Lee, M. R. Sprague, B. J. Sussman, J. Nunn, N. K. Langford, X.-M. Jin, T. Champion, P. Michelberger, K. F. Reim, D. England, D. Jaksch, and I. A. Walmsley, “Entangling Macroscopic Diamonds at Room Temperature,” *Science* **334**, 1253–1256 (2011).
  - [5] Markus Aspelmeyer, Tobias J. Kippenberg, and Florian Marquardt, “Cavity optomechanics,” *Rev. Mod. Phys.* **86**, 1391–1452 (2014).
  - [6] T. P. Purdy, K. E. Grutter, K. Srinivasan, and J. M. Taylor, “Quantum correlations from a room-temperature optomechanical cavity,” *Science* **356**, 1265–1268 (2017).
  - [7] V. Sudhir, R. Schilling, S. A. Fedorov, H. Schütz, D. J. Wilson, and T. J. Kippenberg, “Quantum Correlations of Light from a Room-Temperature Mechanical Oscillator,” *Phys. Rev. X* **7**, 031055 (2017).
  - [8] E. E. Wollman, C. U. Lei, A. J. Weinstein, J. Suh, A. Kronwald, F. Marquardt, A. A. Clerk, and K. C. Schwab, “Quantum squeezing of motion in a mechanical resonator,” *Science* **349**, 952–955 (2015).
  - [9] Ralf Riedinger, Sungkun Hong, Richard A. Norte, Joshua A. Slater, Juying Shang, Alexander G. Krause, Vikas Anant, Markus Aspelmeyer, and Simon Gröblacher, “Non-classical correlations between single photons and phonons from a mechanical oscillator,” *Nature* **530**, 313–316 (2016).
  - [10] Ralf Riedinger, Andreas Wallucks, Igor Marinković, Clemens Löschnauer, Markus Aspelmeyer, Sungkun Hong, and Simon Gröblacher, “Remote quantum entanglement between two micromechanical oscillators,” *Nature* **556**, 473 (2018).
  - [11] C. F. Ockeloen-Korppi, E. Damskägg, J.-M. Pirkkalainen, M. Asjad, A. A. Clerk, F. Massel, M. J. Woolley, and M. A. Sillanpää, “Stabilized entanglement of massive mechanical oscillators,” *Nature* **556**, 478–482 (2018).
  - [12] Yiwen Chu, Prashanta Kharel, Taekwan Yoon, Luigi Frunzio, Peter T. Rakich, and Robert J. Schoelkopf, “Creation and control of multi-phonon Fock states in a bulk acoustic wave resonator,” *Nature* **563**, 666 (2018).
  - [13] L. M. Duan, M. D. Lukin, J. I. Cirac, and P. Zoller, “Long-distance quantum communication with atomic ensembles and linear optics,” *Nature* **414**, 413–418 (2001).
  - [14] Christophe Galland, Nicolas Sangouard, Nicolas Piro,

- Nicolas Gisin, and Tobias J. Kippenberg, “Heralded Single-Phonon Preparation, Storage, and Readout in Cavity Optomechanics,” *Phys Rev Lett* **112**, 143602 (2014).
- [15] P. Grangier, G. Roger, and A. Aspect, “Experimental Evidence for a Photon Anticorrelation Effect on a Beam Splitter: A New Light on Single-Photon Interferences,” *EPL* **1**, 173 (1986).
- [16] Leonard Mandel and Emil Wolf, *Optical Coherence and Quantum Optics* (Cambridge University Press, 1995).
- [17] K. C. Lee, B. J. Sussman, M. R. Sprague, P. Michelberger, K. F. Reim, J. Nunn, N. K. Langford, P. J. Bustard, D. Jaksch, and I. A. Walmsley, “Macroscopic non-classical states and terahertz quantum processing in room-temperature diamond,” *Nat Photon* **6**, 41–44 (2012).
- [18] D. G. England, P. J. Bustard, J. Nunn, R. Lausten, and B. J. Sussman, “From Photons to Phonons and Back: A THz Optical Memory in Diamond,” *Phys. Rev. Lett.* **111**, 243601 (2013).
- [19] Duncan G. England, Kent Fisher, Jean-Philippe W. MacLean, Philip J. Bustard, Rune Lausten, Kevin J. Resch, and Benjamin J. Sussman, “Storage and Retrieval of THz-Bandwidth Single Photons Using a Room-Temperature Diamond Quantum Memory,” *Phys. Rev. Lett.* **114**, 053602 (2015).
- [20] P.-Y. Hou, Y.-Y. Huang, X.-X. Yuan, X.-Y. Chang, C. Zu, L. He, and L.-M. Duan, “Quantum teleportation from light beams to vibrational states of a macroscopic diamond,” *Nat. Commun.* **7**, 11736 (2016).
- [21] Kent A. G. Fisher, Duncan G. England, Jean-Philippe W. MacLean, Philip J. Bustard, Kevin J. Resch, and Benjamin J. Sussman, “Frequency and bandwidth conversion of single photons in a room-temperature diamond quantum memory,” *Nat. Commun.* **7**, 11200 (2016).
- [22] Kent A. G. Fisher, Duncan G. England, Jean-Philippe W. MacLean, Philip J. Bustard, Khabat Heshami, Kevin J. Resch, and Benjamin J. Sussman, “Storage of polarization-entangled THz-bandwidth photons in a diamond quantum memory,” *Phys. Rev. A* **96**, 012324 (2017).
- [23] Hugo Flayac and Vincenzo Savona, “Heralded Preparation and Readout of Entangled Phonons in a Photonic Crystal Cavity,” *Phys. Rev. Lett.* **113**, 143603 (2014).
- [24] V. Caprara Vivoli, T. Barnea, C. Galland, and N. Sangouard, “Proposal for an Optomechanical Bell Test,” *Phys. Rev. Lett.* **116**, 070405 (2016).
- [25] Igor Marinkovic, Andreas Wallucks, Ralf Riedinger, Sungkun Hong, Markus Aspelmeyer, and Simon Gröblacher, “An optomechanical Bell test,” ArXiv180610615 Cond-Mat Physicsphysics Physicsquant-Ph (2018).
- [26] T. von Foerster and R. J. Glauber, “Quantum theory of light propagation in amplifying media,” *Phys. Rev. A* **3**, 1484 (1971).
- [27] N. Bloembergen, *Nonlinear Optics* (W. A. Benjamin, 1965).
- [28] Mark Kasperczyk, Ado Jorio, Elke Neu, Patrick Maletinsky, and Lukas Novotny, “Stokes–anti-Stokes correlations in diamond,” *Opt. Lett.* **40**, 2393 (2015).
- [29] Carlos A. Parra-Murillo, Marcelo F. Santos, Carlos H. Monken, and Ado Jorio, “Stokes anti-Stokes correlation in the inelastic scattering of light by matter and generalization of the Bose-Einstein population function,” *Phys. Rev. B* **93**, 125141 (2016).
- [30] Mikolaj K. Schmidt, Ruben Esteban, Alejandro González-Tudela, Geza Giedke, and Javier Aizpurua, “Quantum Mechanical Description of Raman Scattering from Molecules in Plasmonic Cavities,” *ACS Nano* **10**, 6291–6298 (2016).
- [31] Mark Kasperczyk, Filomeno S. de Aguiar Júnior, Casiano Rabelo, Andre Saraiva, Marcelo F. Santos, Lukas Novotny, and Ado Jorio, “Temporal Quantum Correlations in Inelastic Light Scattering from Water,” *Phys. Rev. Lett.* **117**, 243603 (2016).
- [32] André Saraiva, Filomeno S. de Aguiar Júnior, Reinaldo de Melo e Souza, Arthur Patrocínio Pena, Carlos H. Monken, Marcelo F. Santos, Belita Koiller, and Ado Jorio, “Photonic Counterparts of Cooper Pairs,” *Phys. Rev. Lett.* **119**, 193603 (2017).
- [33] A. Weinstein, C. Lei, E. Wollman, J. Suh, A. Metelman, A. Clerk, and K. Schwab, “Observation and interpretation of motional sideband asymmetry in a quantum electromechanical device,” *Phys. Rev. X* **4**, 041003 (2014).
- [34] Roy J. Glauber, “The Quantum Theory of Optical Coherence,” *Phys. Rev.* **130**, 2529–2539 (1963).
- [35] Mitchell D. Anderson, Santiago Tarrago Velez, Kilian Seibold, Hugo Flayac, Vincenzo Savona, Nicolas Sangouard, and Christophe Galland, “Two-Color Pump-Probe Measurement of Photonic Quantum Correlations Mediated by a Single Phonon,” *Phys. Rev. Lett.* **120**, 233601 (2018).
- [36] A. L. Lacaíta, F. Zappa, S. Bigliardi, and M. Manfredi, “On the bremsstrahlung origin of hot-carrier-induced photons in silicon devices,” *IEEE Transactions on Electron Devices* **40**, 577 (1993).
- [37] P. Sekatski, N. Sangouard, F. Bussières, C. Clausen, N. Gisin, and H. Zbinden, “Detector imperfections in photon-pair source characterization,” *J. Phys. B At. Mol. Opt. Phys.* **45**, 124016 (2012).
- [38] S. Friberg, C. K. Hong, and L. Mandel, “Intensity dependence of the normalized intensity correlation function in parametric down-conversion,” *Opt. Comm.* **54**, 311 (1985).
- [39] Philippe Roelli, Christophe Galland, Nicolas Piro, and Tobias J. Kippenberg, “Molecular cavity optomechanics as a theory of plasmon-enhanced Raman scattering,” *Nat Nano* **11**, 164–169 (2016).
- [40] H. Wang, M. Hofheinz, M. Ansmann, R. C. Bialczak, E. Lucero, M. Neeley, A. D. O’Connell, D. Sank, J. Wenner, A. N. Cleland, and John M. Martinis, “Measurement of the Decay of Fock States in a Superconducting Quantum Circuit,” *Phys. Rev. Lett.* **101**, 240401 (2008).
- [41] M. Brune, J. Bernu, C. Guerlin, S. Deléglise, C. Sayrin, S. Gleyzes, S. Kuhr, I. Dotsenko, J. M. Raimond, and S. Haroche, “Process Tomography of Field Damping and Measurement of Fock State Lifetimes by Quantum Non-demolition Photon Counting in a Cavity,” *Phys. Rev. Lett.* **101**, 240402 (2008).
- [42] Steven Yampolsky, Dmitry A. Fishman, Shirshendu Dey, Eero Hulkko, Mayukh Banik, Eric O. Potma, and Vartkess A. Apkarian, “Seeing a single molecule vibrate through time-resolved coherent anti-Stokes Raman scattering,” *Nat Photon* **8**, 650–656 (2014).
- [43] Philip J. Bustard, Rune Lausten, Duncan G. England, and Benjamin J. Sussman, “Toward Quantum Processing in Molecules: A THz-Bandwidth Coherent Memory for

- Light,” *Phys. Rev. Lett.* **111**, 083901 (2013).
- [44] Philip J. Bustard, Jennifer Erskine, Duncan G. England, Josh Nunn, Paul Hockett, Rune Lausten, Michael Spanner, and Benjamin J. Sussman, “Nonclassical correlations between terahertz-bandwidth photons mediated by rotational quanta in hydrogen molecules,” *Opt. Lett.*, **OL 40**, 922–925 (2015).
- [45] Philip J. Bustard, Duncan G. England, Khabat Heshami, Connor Kupchak, and Benjamin J. Sussman, “Reducing noise in a Raman quantum memory,” *Opt. Lett.*, **OL 41**, 5055–5058 (2016).
- [46] Felix Benz, Mikolaj K. Schmidt, Alexander Dreismann, Rohit Chikkaraddy, Yao Zhang, Angela Demetriadou, Cloudy Carnegie, Hamid Ohadi, Bart de Nijs, Ruben Esteban, Javier Aizpurua, and Jeremy J. Baumberg, “Single-molecule optomechanics in “picocavities”,” *Science* **354**, 726–729 (2016).
- [47] Anna Lombardi, Mikolaj K. Schmidt, Lee Weller, William M. Deacon, Felix Benz, Bart de Nijs, Javier Aizpurua, and Jeremy J. Baumberg, “Pulsed Molecular Optomechanics in Plasmonic Nanocavities: From Non-linear Vibrational Instabilities to Bond-Breaking,” *Phys. Rev. X* **8**, 011016 (2018).
- [48] Ado Jorio, Mark Kasperczyk, Nick Clark, Elke Neu, Patrick Maletinsky, Aravind Vijayaraghavan, and Lukas Novotny, “Optical-Phonon Resonances with Saddle-Point Excitons in Twisted-Bilayer Graphene,” *Nano Lett.* **14**, 5687–5692 (2014).
- [49] Tao Jiang, Hao Hong, Can Liu, Wei-Tao Liu, Kaihui Liu, and Shiwei Wu, “Probing Phonon Dynamics in Individual Single-Walled Carbon Nanotubes,” *Nano Lett.* **18**, 2590–2594 (2018).

## Acknowledgements

Funding for this research was provided by the Swiss National Science Foundation, project numbers PP00P2-170684. KS acknowledges support from the Swiss National Science Foundation, project 200021-162357. VS is supported by a Swiss National Science Foundation fellowship (P2ELP2\_178231).